Ion Binding and Selectivity of the Na+/H+ Antiporter MjNhaP1 from Experiment and Simulation

Judith Warnau,[†,‡,#] David Wöhlert,[¶,#] Kei-ichi Okazaki,[§] Özkan Yildiz,[¶] Ana P. Gamiz-Hernandez,[‡,ll] Ville R. I. Kaila,*[,‡,ll] Werner Kühlbrandt,*[,¶] and Gerhard Hummer*[,†,⊥]

[†]Department of Theoretical Biophysics, Max Planck Institute of Biophysics, 60438 Frankfurt am Main, Germany

[‡]Department Chemie, Technische Universität München, 85748 Garching, Germany

[¶]Department of Structural Biology, Max Planck Institute of Biophysics, 60438 Frankfurt am Main, Germany
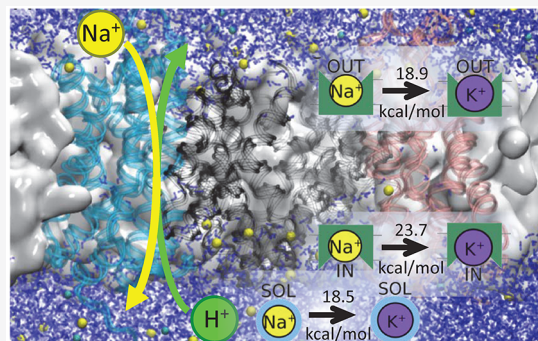
[§]Department of Theoretical and Computational Molecular Science, Institute for Molecular Science, National Institutes of Natural Science, Okazaki, 444-8585, Japan

[ll]Department of Biochemistry and Biophysics, Stockholm University, 10691 Stockholm, Sweden

[⊥]Institute of Biophysics, Goethe University Frankfurt, 60438 Frankfurt am Main, Germany

S Supporting Information

ABSTRACT: Cells employ membrane-embedded antiporter proteins to control their pH, salt concentration, and volume. The large family of cation/proton antiporters is dominated by Na+/H+ antiporters that exchange sodium ions against protons, but homologous K+/H+ exchangers have recently been characterized. We show experimentally that the electroneutral antiporter NhaP1 of *Methanocaldococcus jannaschii* (MjNhaP1) is highly selective for Na+ ions. We then characterize the ion selectivity in both the inward-open and outward-open states of MjNhaP1 using classical molecular dynamics simulations, free energy calculations, and hybrid quantum/classical (QM/MM) simulations. We show that MjNhaP1 is highly selective for binding of Na+ over K+ in the inward-open state, yet it is only weakly selective in the outward-open state. These findings are consistent with the function of MjNhaP1 as a sodium-driven deacidifier of the cytosol that maintains a high cytosolic K+ concentration in environments of high salinity. By combining experiment and computation, we gain mechanistic insight into the Na+/H+ transport mechanism and help elucidate the molecular basis for ion selectivity in cation/proton exchangers.

INTRODUCTION

Sodium/proton (Na+/H+) antiporters or exchangers (NHE) are membrane proteins involved in the control of cellular pH, salt concentration, and volume.[1] In reflection of these essential functions, antiporters are present in all branches of life. Mutations in the genes coding for human Na+/H+ exchange (NHE) proteins are linked to epilepsy, autism, diabetes, and other diseases.[2,3] Functional similarities and sequence homology in the cation−proton antiporter (CPA) family have motivated extensive studies of microbial antiporters to gain a mechanistic understanding of the ion-exchange mechanism and to shed light on the molecular effects of disease-associated mutations in human NHEs.

Na+/H+ antiporters are secondary-active transporters. In a tightly coupled exchange process, they employ an electrochemical gradient of one ion species across a membrane to drive the thermodynamically unfavorable transport of another ion. To this end, the Na+/H+ antiporters employ conformational transitions between two alternate access states,[4,5] in which the ion binding sites face opposite sides of the membrane. If transitions between the inward-open and outward-open access states are feasible only with bound Na+ and/or H+, conformational switching between these states results in selective ion exchange.[4,5]

Atomic structures of Na+/H+ antiporters have been resolved for two bacterial systems, NhaA from *Escherichia coli* (EcNhaA)[6] and NapA from *Thermus thermophilus* (TtNapA),[7] and for two archaeal systems, NhaP from *Pyrococcus abyssi* (PaNhaP)[8] and NhaP1 from *Methanocaldococcus jannaschii* (MjNhaP1).[9] NhaA and NapA are members of the CPA2 family with a transport stoichiometry of one Na+ ion per two H+. The structures of two electroneutral CPA1-family antiporters with a Na+/H+ transport stoichiometry of 1:1, PaNhaP and MjNhaP1, were resolved with X-ray crystallography in inward-open states.[9] By using 2D-electron crystallography, MjNhaP1 was also resolved in an outward-open state.[9] The archaeal members of the CPA1-family are thought to be closely related to human NHEs because of the similarities in

the transport stoichiometry and direction. Also in terms of their sequence, eukaryotic antiporters are slightly closer to archaeal antiporters than to bacterial antiporters.[10]

MjNhaP1 is believed to maintain the intracellular pH by actively transporting protons out of the cell by using an inward Na$^+$ gradient between the saline environment and the cell interior.[7,9] Electrophysiology measurements confirmed the alternating-access model and the competition between H$^+$ and Na$^+$ for the same binding site.[11] Important mechanistic insight into the ion exchange mechanism was also obtained from combined structural studies and molecular dynamics (MD) simulations of the electrogenic antiporters EcNhaA[12] and TtNapA.[7] For PaNhaP, we recently resolved the Na$^+$ and H$^+$ transport cycle by transition-path sampling.[13] In molecular dynamics trajectories of ion exchange without bias force, an elevator-like vertical motion of the transporter domain over 3–4 Å was associated with the opening and closing of a hydrophobic gate.

M. jannaschii is an archaeon living near submarine hydrothermal vents. Maintaining a high cytosolic K$^+$ concentration in a sea water environment with abundant Na$^+$ thus requires high selectivity for Na$^+$ over K$^+$. However, several antiporters homologous to MjNhaP1 have been found to exchange K$^+$ ions.[14−16] This finding raises the question whether MjNhaP1 is indeed selective for Na$^+$ and, if so, which molecular determinants are responsible for selectivity.

To address these questions, we characterize here the ion selectivity of MjNhaP1 by experiments and atomistic MD simulations using classical and hybrid quantum mechanics/classical mechanics (QM/MM) representations. Taking advantage of the recent crystal structure in an inward-open state,[9] and the electron density map from a recent electron microscopy (EM) experiment,[9] we create an atomistic model of the outward-open state. Using free energy calculations, we determine the difference in free energy for the binding of K$^+$ and Na$^+$ ions in both inward-open and outward-open states. We also identify residues that contribute to ion selectivity on the basis of sequence variations and our MD simulations. We characterize the effects of different amino acids and interactions on ion binding using combined free energy calculations and site-directed mutagenesis experiments. We conclude by relating our findings to putative physiological functions of MjNhaP1.

■ METHODS

Purification, Reconstitution, and Transport Assays. To initiate transport, proteoliposomes were diluted 1:1000 into activity buffer (10 mM choline citrate buffer, 2 μM acridine orange). Fluorescence measurements were performed at an excitation wavelength of 495 nm, by monitoring emission at 530 nm to detect a pH gradient across the membrane, indicative of cation/proton exchange. Proton gradients were dissipated by the addition of $(NH_4)_2SO_4$ to a concentration of 25 mM at the end of the experiment. To compare the ion selectivity with the same batch of liposomes, transport was initiated with sodium-loaded liposomes, as described above. Once the initial reaction reached equilibrium, KCl or NaCl was added to the reaction buffer to a concentration of 5 mM, resulting in reverse transport when the cation serves as a substrate for the transporter.

MD Simulations of the Inward-Open State. The crystal structure of MjNhaP1 in an inward-open dimeric state (PDB ID: 4CZB)[9] was embedded into a 1-palmitoyl-2-oleoyl-phosphatidylethanolamine (POPE) lipid bilayer and solvated with 150 mM NaCl in a box of size 156 × 126 × 105 Å^3. The protonation states of ionizable residues were assigned based on electrostatic calculations using PROPKA.[17,18] On the basis of these calculations, Asp-93, Glu-344, and Glu-401 were modeled in their protonated state in both monomers. The residues forming the ion-binding site are conserved between PaNhaP and MjNhaP1. A superposition of the crystallographically resolved binding site of PaNhaP[8] allowed us to place the Na$^+$ ion. The subsequent MD simulations relaxed the coordinating residues and resulted in stable ion binding. In some instances, ion binding occurred spontaneously from the bulk solution, corroborating the conservation of the ion binding site between PaNhaP and MjNhaP1. Molecular dynamics simulations were performed with NAMD2.9/2.10/2.11[19] using the CHARMM36 force field.[20,21] The force field parameters for Na$^+$, K$^+$, and Cl$^−$ ions were obtained from refs 22 and 23. The temperature was kept constant at 310 K with Langevin dynamics using a 2 fs integration time step. The pressure was held at 1 atm using a Langevin piston.[24] Long-range electrostatic interactions were treated with the particle-mesh Ewald approach.[25] Following energy minimization and a brief relaxation for 1.5 ns, the inward-open state was simulated for 1 μs.

Molecular Dynamics Flexible Fitting and MD Simulations of the Outward-Open State. We used molecular dynamics flexible fitting (MDFF)[26] to fit the inward-open crystal structure of MjNhaP1 (PDB ID: 4CZB[9]) into the EM map of 2D crystals of the protein in an outward-open state.[9] The initial structure in the MDFF runs was aligned to the outward-open structure (PDB ID: 4D0A), which had previously been fitted manually into the EM map.[9] We set the MDFF scaling factor[26] to ξ = 0.3 kcal mol^{-1}. To maintain the secondary structure, harmonic restraints were applied to ϕ and ψ angles of residues in helices or sheets with a spring constant k_μ = 200 kcal mol^{-1} rad^{-2}, and to their backbone hydrogen bonds with a spring constant k'_μ = 200 kcal mol^{-1} Å^{-2}, with additional terms ensuring proper peptide stereochemistry. After flexible fitting for 2 ns, we performed 200 steps of energy minimization. During the MDFF simulation, the cross-correlation coefficient of calculated and measured maps increased from 0.32 to 0.79. The resulting transporter dimer structure was embedded into a POPE lipid bilayer and solvated with 150 mM aqueous NaCl solution. The initial box size was 161 × 130 × 98 Å^3. The outward-open conformation of PaNhaP was obtained by targeted MD using the outward-open model of MjNhaP1 described here as a reference.[13] The total number of atoms in the simulation box was approximately 177,000. This system was equilibrated for 68 ns with restraints to the final structure of the MDFF simulations that were removed in subsequent 90 ns free MD simulations. We then simulated the outward-open state of MjNhaP1 for 1 μs at equilibrium and without restraints.

MD with Bound Potassium. We simulated the MjNhaP1 dimer both in inward-open and outward-open states with K$^+$ bound instead of Na$^+$. After 100 ns of equilibrium MD simulation of MjNhaP1, we substituted the bound Na$^+$ by K$^+$ in both monomers, but kept the NaCl solution environment. We then performed 1 μs of equilibrium MD simulation in the inward-open state and 500 ns in the outward-open state with bound K$^+$ in the binding sites.

QM/MM Descriptions of Ion Binding. The ion-binding site of the antiporter MjNhaP1 was also modeled using QM/

MM simulations of a monomeric model of MjNhaP1. A reduced model of MjNhaP1 with approximately 10 000 atoms and a 5-Å water and ion layer was constructed based on the structure obtained after a 100 ns of classical unrestrained MD simulations described above. The QM region comprised the bound alkali metal ion (Na^+ or K^+), the surrounding residues forming the ion binding site[8] (Thr-131, Asp-132, Ser-157, Asn-160, Asp-161), and three directly coordinated water molecules. The QM region was truncated using link atoms, introduced between the QM and MM regions (Figure S1). The B3LYP[27,28] hybrid functional was used together with def2-SVP and def2-TZVP basis sets (for Na^+/K^+)[29] to model the QM region. The remaining system was treated classically (MM) with the CHARMM27 force field.[30,31] In total, four QM/MM simulations, 7 ps each, were performed at constant temperature (T = 310 K) with a 1 fs integration step, starting from the inward-open and outward-open states with Na^+ and K^+ bound at the binding site, respectively. All QM/MM simulations were performed using the TURBOMOLE-CHARMM interface.[31−34] Here, we use relatively short QM/MM simulations to probe the geometry of the ion-binding sites with chemical detail. With much longer simulations, it would be possible to estimate quantum chemical corrections to the relative ion binding affinities.[35] Lev et al.[35] examined dependences on the basis set and the size of the QM and MM regions. During our QM/MM simulations, the three water molecules in the QM region stayed close to the bound ion.

Calculations of Ion-Binding Free Energies. Alchemical free energy perturbation (FEP) calculations were performed to estimate free energy differences of Na^+ and K^+ binding from the cytosolic and extracellular sides, respectively. The alchemical transformations between Na^+ and K^+ ions were performed using a single-topology approach. To this end, the Lennard-Jones parameters of the two ions were interconverted in 41 steps, using a linear interpolation parametrized with end points corresponding to Na^+ (λ = 0) and K^+ (λ = 1). The charge of the ion was kept constant during the transformation process. In the alchemical free energy simulations, the ion remained bound, eliminating the need to apply a restraining potential. In each window, the system was initially relaxed for 0.5 ns, followed by a production run of 1 ns. After relaxation of the K^+-bound state (λ = 1), the K^+ ion was transformed back to Na^+. The forward ($Na^+ \rightarrow K^+$) and reverse paths ($K^+ \rightarrow Na^+$) followed the same protocol. For configurations saved at intervals of 0.2 ps, the energy differences to the end points and the respective intermediate states were determined. From these energy differences, the free energy differences were calculated using the mBAR formalism.[36] The free energies were also calculated using data only from the forward and reverse paths to test for possible hysteresis effects. Statistical uncertainties in the free energies were estimated based on 10 independent forward and reverse pathway calculations. The same FEP protocol was used to calculate the difference in ion-solvation free energy in bulk aqueous solution. To this end, a single ion was introduced in a water box of size 40 × 40 × 40 Å[3]. Since the charge state does not change during the transformation between Na^+ and K^+, finite-size effects are kept at a minimum,[37] except for possible dielectric effects that could arise from the vicinity to the low-dielectric protein interior and the membrane environment.[38,39]

FEP calculations for the outward-open state were performed on MjNhaP1 chain B (PDB ID: 4CZB[9]), where the ions are coordinated fully in both access states. For the inward-open state, FEP calculations were performed on MjNhaP1 chain A (PDB ID: 4CZB[9]). In contrast to its homologue PaNhaP,[8] transport of substrates by MjNhaP1 follows Michaelis—Menten kinetics.[9] The lack of cooperativity suggests that the two monomers operate independently, but dimer formation might, nevertheless, be necessary to stabilize the transporter. As was done for *E. coli* NhaA,[40] which functions as a monomer but dimerizes to increase stability, monomerization of the transporter would be required to exclude a functional role of the dimer.

All structures were visualized using Visual Molecular Dynamics (VMD).[41] Sequences were aligned with the multiple sequence alignment web server PSI/TM-Coffee[42,43] with the transmembrane option for the sequence type and the UniRef100 option for the homology extension. Sequence alignments were represented with jalview.[44]

RESULTS

Experimental Characterization of MjNhaP1 Ion Selectivity. We determined the ion selectivity of MjNhaP1 by reconstituting the transporter into liposomes, measuring the transport activity by adding external Na^+ or K^+ and monitoring the fluorescence as a reporter on pH. In contrast to a Na^+ pulse, which triggers a clear proton influx, addition of K^+ to the previously established transporter equilibrium does not induce a shift toward a new equilibrium (Figure 1A). To probe the dependence on the ion concentration, we also performed the experiments by loading the liposomes with either 200 mM NaCl or KCl. Also in these control experiments, the cation-mediated proton influx was only detected with Na^+ but not with K^+-loaded proteoliposomes (Figure 1B). Taken together, the experiments demonstrate that K^+ does not serve as a substrate for WT MjNhaP1.

Ion Binding to MjNhaP1 in the Inward-Open and Outward-Open States. *Dynamics of the Inward-Open and Outward-Open Access States.* To obtain molecular insight into Na^+ binding, we performed a 1-μs MD simulation of the inward-open state of MjNhaP1. In this simulation, the ion-binding sites of both monomers remained continuously accessible to water molecules and ions from the inside of the cell. Figure 2 shows root-mean-square deviation (RMSD) profiles relative to the inward-open reference crystal structure. In the simulation of the inward-open state, we observed a stable RMSD of about 2 Å for both chains A and B. The bound Na^+ ions were coordinated by Thr-131, Ser-157, Asn-160, and Asp-161 in both monomer chains (Figures 3 and 4), consistent with previous work on MjNhaP1[9] and EcNhaA.[12] The MD simulation, initiated from the crystal structure, thus captured key features of a physiologically meaningful inward-open state.

Next, we performed a 1-μs unrestrained equilibrium MD simulation of MjNhaP1 in the outward-open state starting from the MDFF-refined model. During the simulation, we observed persistent Na^+ binding in chain B (Figures 4 and 5), and repeated Na^+ binding and unbinding events in chain A (Figure 5). Chain B moved further away from the inward-open reference than chain A, with RMSD values of about 4 and 3 Å, respectively. In light of the lower RMSD and the ion-binding results described below, in chain A the transition to a fully outward-open conformation appears to be incomplete. Our structural model of the outward-open state has, as previously suggested[9] and functionally required, ion binding sites accessible only from the outside.
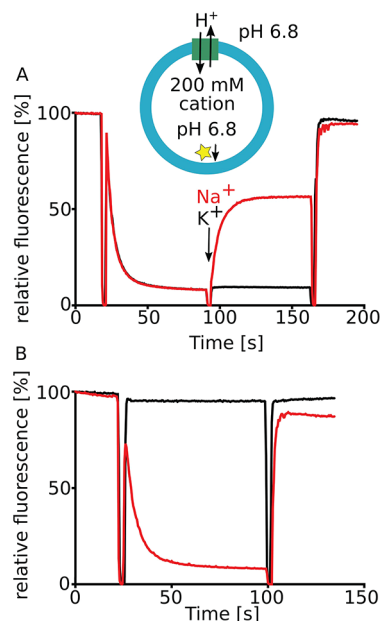
Figure 1. Experimental determination of MjNhaP1 ion selectivity. (A) Na$^+$-loaded proteoliposomes were diluted in reaction buffer, resulting in a drop of fluorescence due to proton influx mediated by MjNhaP1 transport activity. After initial equilibration, addition (arrow) of Na$^+$ (red) to a concentration of 5 mM resulted in reverse transport of protons and an increase in fluorescence. Addition of K$^+$ to the same concentration (black) did not shift the transport equilibrium. (B) Proteoliposomes were loaded with either 200 mM Na$^+$ (red) or K$^+$ (black) and diluted into reaction buffer. Whereas a pH difference built up in Na$^+$-loaded liposomes, the fluorescence remained constant for the K$^+$-loaded liposomes. Thus, even at higher concentrations, K$^+$-driven proton influx was not detectable for WT MjNhaP1. The measured acridine orange fluorescence reports on the change in pH inside the proteoliposomes.

As a basis for the subsequent explorations of Na$^+$ selectivity against K$^+$, we performed MD simulations of inward- and outward-open states with bound K$^+$. Irrespective of the type of the bound ion, Na$^+$ or K$^+$, the ion-binding sites of the outward-open state were more exposed to solvent than those of the inward-open state (Figure 4). In particular, Na$^+$ has approximately 3 water ligands in the outward-open state compared to approximately 1 in the inward-open state (Figure 5). In the inward-open state, both protomers persistently accommodated Na$^+$, whereas K$^+$ bound stably only to chain B and dissociated from chain A. The larger size of the K$^+$ ion, as compared to Na$^+$, induced conformational changes in the coordinating ligands. In addition to longer coordination distances to K$^+$ (Figure S2, Table S1), we noticed that the Ser-157 hydroxyl side chain pointed for most of the simulation time away from Na$^+$, but coordinated K$^+$ (Figure S2). This difference in ion coordination pointed to Ser-157 as a possible determinant for ion selectivity, encouraging us to probe the effect of removing the serine side chain by mutation. The ion binding modes seen in the QM/MM and classical MD simulations are nearly identical, including the coordination geometries and bond distances (Table S1).

Occupancy of Ion Binding Sites. Having established the binding mode of Na$^+$ and K$^+$ ions in the inward-open and outward-open states, we characterized the ion occupancy of the binding sites during the MD simulations. Na$^+$ binds in a stable conformation to the binding sites of chains A and B in
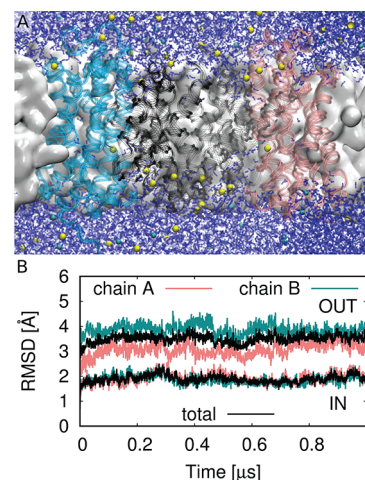

Figure 2. Atomistic MD simulation of MjNhaP1 embedded in a POPE lipid membrane. (A) Snapshot of inward-open conformational state after 1 μs of MD simulation. The six-helix bundle domains of chains A and B are shown in coral and cyan, respectively. The interface domains of chains A and B are shown in gray and black, respectively. The membrane is represented as a white surface. Water and ions are drawn as sticks and spheres, respectively (Na$^+$, yellow; Cl$^-$, cyan). (B) RMSD calculated for the 1 μs MD simulations of the inward-open (lower curves labeled IN) and outward-open (upper curves labeled OUT) conformational states in reference to the inward-open crystal structure. Results are shown for chain A (coral), chain B (cyan), and for both monomers ("total", black). Only the backbone atoms of the helices were taken into account in the RMSD calculations.
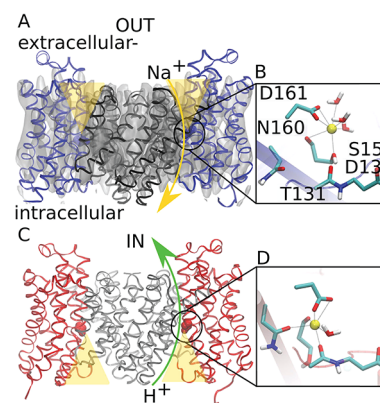

Figure 3. MjNhaP1 structure and function. (A) Outward-open structure of MjNhaP1 dimer after 1 μs MD simulation. The binding site domains and interface domains of chains A and B are shown in blue and black, respectively. Schematic illustration of the Na$^+$ transport direction from the outside to the inside of the cell (yellow arrow) in chain B. The water and ion accessibility of the binding sites toward the outside is indicated by yellow transparent triangles. (B) Close-up view of the Na$^+$ binding site of chain B (Thr-131, Asp-132, Ser-157, Asn-160, and Asp-161), as viewed from the outside. (C) Inward-open structure of MjNhaP1 dimer after 1 μs of MD simulation. The binding site domains and interface domains of the two monomers are shown in red and gray, respectively. Schematic illustration of the proton transport direction from the inside to the outside of the cell (green arrow) in chain A. The water and ion accessibility of the binding sites toward the inside is indicated by yellow transparent triangles. (D) Zoom-in on the Na$^+$ binding site of chain A (Thr-131, Asp-132, Ser-157, Asn-160, and Asp-161), as viewed from the outside.
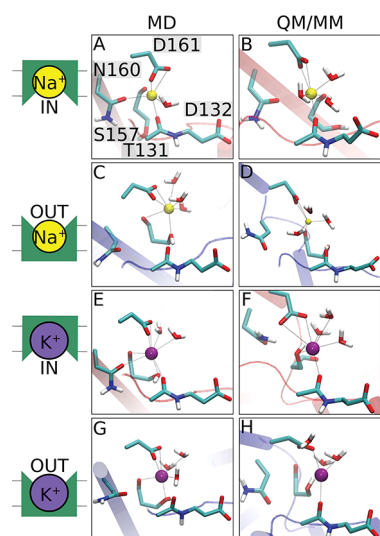
Figure 4. Comparison of the ion-binding sites from MD simulations (left) and QM/MM simulations (right) with bound Na$^+$ and K$^+$ in inward-open and outward-open conformational states. Residues Thr-131, Asp-132, Ser-157, Asn-160, and Asp-161 are shown. (A, B) Chain A in the inward-open state with bound Na$^+$. (C, D) Chain B in the outward-open state with bound Na$^+$. (E, F) Chain B in the inward-open state with bound K$^+$. (G, H) Chain B in the outward-open state with bound K$^+$. The number of water ligands shown in the representations of the binding sites from MD simulations (left) reflect the most probable coordination number (see Figure 5). In the QM/MM simulations (right; see Methods), the three closest water molecules are included in the QM region and shown here.

the inward-open state (Figure 5B). By contrast, in the outward-open state the binding sites of both chains showed repeated binding and unbinding events involving different Na$^+$ ions (Figure 5, Figure S3). In the outward-open binding site of chain B, the Na$^+$ ions remained well-coordinated, forming direct interactions with the carboxylate group of Asp-161 as well as the carbonyl and side chain oxygen atoms of Ser-157. By contrast, in chain A the Na$^+$ ions interacted directly with Asp-161, but not Ser-157 or Thr-131 (Figure 5D, Figure S4).

We found that K$^+$ remained bound to chain B during the entire MD simulation in both the inward-open and outward-open states. By contrast, in both access states the bound K$^+$ ion in the binding site of the A chain eventually escaped into the bulk (Figure 5E,G). In chain A of the outward-open state, the K$^+$ ion formed tight interactions only with Asp-161. K$^+$ release thus appears to be a result of these overall tenuous interaction. The K$^+$ ion escaped from chain A also in the inward-open state, despite a tight initial coordination by Asp-161, Ser-157, and Thr-131 (Figure S2). During the subsequent MD simulation, several Na$^+$ ions approached the empty binding site from the bulk, forming initial contacts with Asp-161 (Figure 5F,H and Figure S4), but did not bind strongly. The escape of K$^+$ and the absence of complete Na$^+$ ion rebinding indicate that the small structural differences between chains A and B in our model structure persist on the simulation time scale and result in a lower ion-binding affinity of chain A. It appears that chain A did not fully complete the transition to an outward-open state. Indeed, the RMSD profiles in Figure 2 place chain A closer to an inward-open state than chain B,
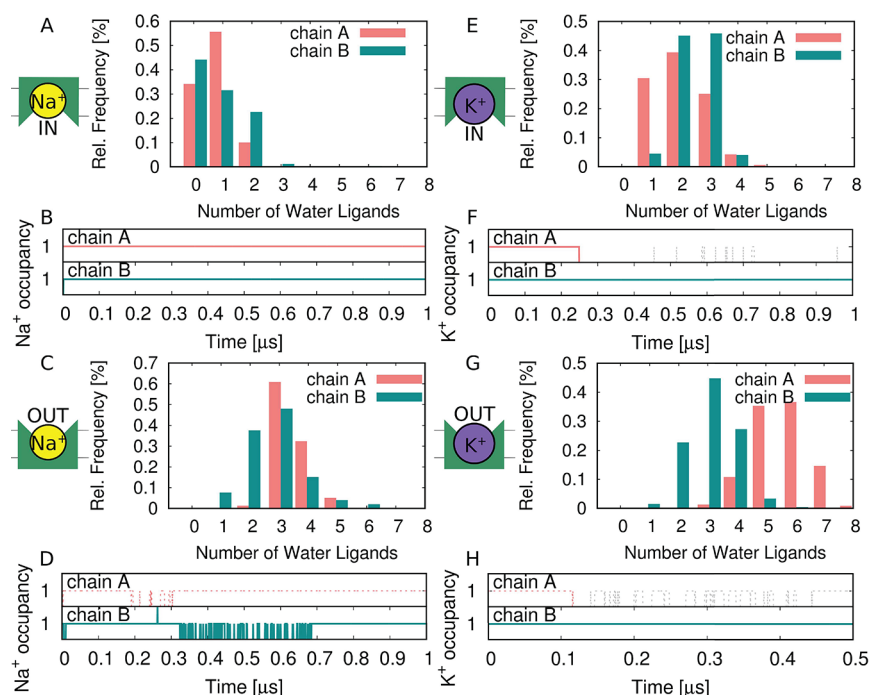

Figure 5. Ion and water occupancy of the binding sites from MD simulations. Histograms show relative frequencies of the number of water ligands coordinating the bound ion in chains A and B (coral and cyan, respectively), with Na$^+$ bound in the inward-open state (A) and the outward-open state (C); with K$^+$ bound in the inward-open state (E) and the outward-open state (G). Water molecules are considered ligands if their oxygen atom is within 2.8 and 3.5 Å of Na$^+$ and K$^+$, respectively. Ion occupancy of the binding sites of chain A and chain B in coral and cyan, respectively, in the inward-open state (B) and the outward-open state (D) with bound Na$^+$, and in the inward-open state (F) and outward-open state (H) with bound K$^+$. Dashed lines indicate that the ion has only contact to Asp-161 at the entry of the ion-binding site and does not fully occupy the binding pocket. Gray dashed lines indicate that Na$^+$ comes close to Asp-161 of chain A in inward-open and outward-open simulations in which originally a K$^+$ ion occupied the binding site (F, H). Ions are considered bound within 4.5 Å of Asp-161.

which may be responsible for the weak ion-binding affinity of chain A in the outward-open state (Figure 5).

Hydration of Bound Ions. We next quantified water molecules coordinating the ions during the MD simulations. We found that the Na$^+$ ions in the inward-open and outward-open states bound to 1 ± 1 and 3 ± 1 coordinating water ligands, respectively, suggesting that the Na$^+$ ions are nearly saturated by interactions with the protein residues in the inward-open binding site, but require additional ligands in the outward-open state.

The K$^+$ ion bound to chain A in the inward-open state had 2 ± 1 additional water ligands, suggesting that the K$^+$ ion is well coordinated by residues in the binding pocket. By contrast, the K$^+$ ion in the outward-open state of chain A formed contacts with only Asp-161 and with 5−6 water ligands, suggesting weak protein interactions that leave the K$^+$ ion exposed to solvent. An incomplete transition of chain A to an outward-open state, as indicated by the RMSD profiles in Figure 2, may be responsible for the weak ion-binding affinity of chain A in the outward-open state (Figure 5). In chain B, we observed a similar trend as for Na$^+$ binding to inward-open and outward-open states. In the inward-open state, the K$^+$ ion coordinated 2−3 water ligands, whereas in the outward-open state, we observed 3 ± 1 water contacts (Figure 5E,G). The different behavior for the two chains are likely the result of subtle differences in the structure that have not relaxed on the simulation time scale. A quantification of the contribution of hydration to the ion binding affinity and to ion selectivity would require free energy calculations in which the hydration number is explicitly controlled, as was done, for instance, in calculations of ion-channel conductance.[45]

Free Energy Calculations of Ion Selectivity. To quantify ion selectivity, we calculated the differences in the ion-binding free energies of Na$^+$ and K$^+$ ions in the inward-open and outward-open states (Figure 6; Tables S3 and S4). In aqueous solution, we obtained a difference in solvation free energy between Na$^+$ and K$^+$ of $\Delta G^{Sol}(Na^+ \rightarrow K^+)$ = 18.459 ± 0.002 kcal mol^{-1}, which compares well to previous computational and experimental free energy estimates of 18.1 kcal mol^{-1}[23] and 17.5 kcal mol^{-1},[46] respectively. In the inward-open state, we obtained $\Delta G^{In}(Na^+ \rightarrow K^+)$ = 23.7 ± 0.3 kcal mol^{-1}, whereas in the outward-open state $\Delta G^{Out}(Na^+ \rightarrow K^+)$ = 18.9 ± 0.1 kcal mol^{-1}. By subtracting the bulk value from these two differences, we estimate that in the inward-open state Na$^+$ binding is favored over K$^+$ binding by 5.2 ± 0.3 kcal mol^{-1}. In the outward-open state, we estimate a smaller free energy difference of 0.4 ± 0.1 kcal mol^{-1} in favor of Na$^+$. Overall, these findings suggest that Na$^+$ is preferred over K$^+$, with possible functional implications of the selectivity difference in the two access states discussed below.

Molecular Contributors to Ion Selectivity. To identify the sequence and structural features responsible for the preferential Na$^+$ binding to MjNhaP1, we examined the effect of mutations in the binding site on the ion selectivity. We identified key amino acids from sequence conservation (Figure S5) of MjNhaP1 and homologous antiporters with known ion selectivity. We divided the sequences into three groups using (1) three transporters of known structure and selectivity for Na$^+$ (PaNhaP, EcNhaA, TtNapA),[6,7,9] (2) three transporters selective for both Na$^+$ and K$^+$ (VcNhaP1, ScNHX1, AtNHX1),[1,14] and (3) three antiporters with K$^+$ selectivity (VcNhaP2, TaNHX2, EcNhaP2).[15,47,48] The first and second group of the Na$^+$ selective and Na$^+$ and K$^+$-selective antiporters
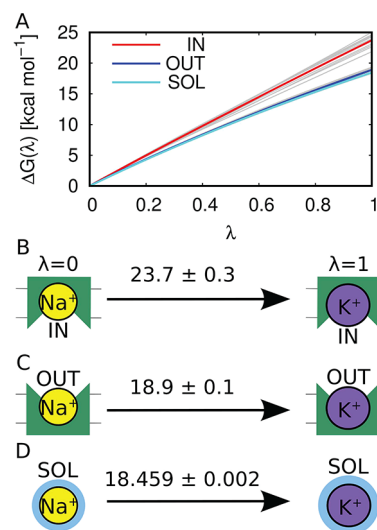

Figure 6. Ion selectivity. (A) Free energy of alchemical transformation as a function of the coupling parameter λ interpolating between Na$^+$ ($\lambda = 0$) and K$^+$ ($\lambda = 1$). Free energy profiles are shown for the inward-open state of MjNhaP1 (red), for the outward-open state (dark blue), and for aqueous solution (cyan), respectively. The free energies were estimated from 10 independent forward and reverse runs (gray). (B−D) Overall free energy differences in kcal mol^{-1} between K$^+$ and Na$^+$ with standard errors of the mean from 10 independent free energy estimates in the inward-open state (B), in the outward-open state (C), and in water (D).

were classified to the first clade of NhaP-I/NHE in the phylogenetic tree,[16] whereas the third group belongs to the third clade of NhaP-II K$^+$-specific antiporters.

The residues directly coordinating the cations are conserved (Thr-131, Asp-161) or partially conserved without clear pattern correlated with the selectivity (Ser-157, Asn-160). However, the amino acid composition in the second shell around the ion-binding site is quite variable without clear patterns for Na$^+$ and K$^+$ selectivity (SI Table S5; see also ref 16 for an extensive analysis). On this basis, we considered A130S, P133S, S157G, and P162A as possible substitutions to enhance the K$^+$ selectivity. For instance, Ala-130 is conserved in the group of Na$^+$-selective antiporters considered here, whereas a serine residue is found at this position in two out of three K$^+$-selective antiporters (Figure S5), consistent with the results of an extensive sequence analysis.[16] With the aim of reducing the charge density at the binding site, as another possible factor to achieve K$^+$ selectivity, we also considered the D161N and D132N substitutions.

In the inward-open state, the effects of these mutations on the free energy (Figure 7A) varied from +2 kcal mol^{-1} to −0.5 kcal mol^{-1}, weakening or strengthening the Na$^+$ preference over K$^+$ relative to WT (Figure 7B; Table S5). We predict the largest shift toward a K$^+$ selectivity for the mutations A130S and P162A, weakening the Na$^+$ affinity relative to K$^+$ by +2 kcal mol^{-1} and +0.8 kcal mol^{-1}, respectively, compared to WT. In the double mutant (A130S/P162A), the calculated effect on the ion selectivity is nearly additive, resulting in a free energy shift of +2.5 kcal mol^{-1}. A major reason for the stabilizing effect of A130S is that the hydroxyl group of the serine interacts with K$^+$. During the alchemical transformations, this contact formed already at intermediate λ-values, as the ion became more similar to K$^+$. On the reverse path, when the ion transforms back to Na$^+$, the interaction is lost (Figure 7C,D).
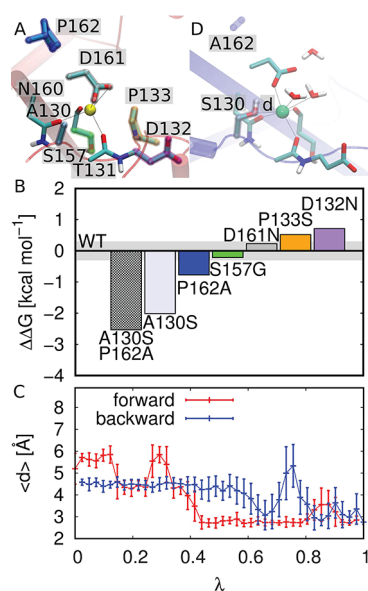
Figure 7. Effect of mutations on ion selectivity of MjNhaP1 in the inward-open state. (A) Binding site of chain A in the inward-open state indicating the mutated residues by colored outlines (A130S, D132N, P133S, S157G, D161N, P162A). (B) Difference in free energy $\Delta\Delta G(Na^+ \rightarrow K^+)$ in kcal mol^{-1} from alchemical transformations for the different mutants in reference to the free energy difference of Na$^+$ and K$^+$ in the WT protein. (C) Average and standard deviation (error bars) of the distance d between the bound ion and the oxygen atom of the hydroxyl group of the Ser-130 in the A130S/P162A double mutant for different values of λ (red, forward transformation; blue, reverse transformation). (D) Snapshot of the binding site during the alchemical transformation of Na$^+$ to K$^+$ in the double mutant A130S/P162A. The mean distance between the bound ion and the oxygen atom of the hydroxyl group of the Ser-130 in each simulation window is indicated as $\langle d \rangle$.

A possible explanation for the relative stabilization of K$^+$ over Na$^+$ by the P162A mutation is a slight increase in the number of water molecules coordinating the ions as a result of a more open binding site (Figure S6, Table S6). In the 1-μs MD simulation of the inward-open WT with bound Na$^+$, we found that on average 1.53 ± 0.58 (Table S2) water ligands coordinated the bound Na$^+$ ion, and 2.50 ± 0.67 water molecules coordinated the bound K$^+$ ion in chain B (Table S2). Our finding that the double mutant (A130S/P162A) shows a significantly lower Na$^+$ selectivity is consistent with the sequence signatures associated with Na$^+$ and K$^+$ selectivity (Figure S5).

To assess the functional impact of these mutations, we convert the free energy differences into concentration ratios at which K$^+$ could outcompete Na$^+$. In the inward-open state of the WT protein, the free energy difference of $\Delta\Delta G^{In} = 5.3$ kcal mol^{-1} would require a 4600-fold excess in K$^+$ concentration over Na$^+$ at $T = 310$ K. In the double mutant (A130S/P162A), this concentration ratio reduces to 80, and thus remains rather large, despite the 2.5 kcal mol^{-1} shift in free energy.

This extreme Na$^+$ selectivity of MjNhaP1 was confirmed by experimental measurements. We performed transport measurements with the MjNhaP1 double mutants A130S/P133A and A130S/P162A (Figure S7), the former also being independently proposed as a possible K$^+$-selective variant on the basis of a phylogenetic analysis.[16] First, we determined whether the addition of Na$^+$ or K$^+$ was able to shift the transport equilibrium. Similar to the WT MjNhaP1, we observed no

change in fluorescence upon addition of K$^+$. By contrast, Na$^+$ showed a clear effect. Given the 80-fold preference of Na$^+$ over K$^+$ for the A130S/P162A double mutant based on the free energy calculations, we performed another experiment in which the proteoliposomes were loaded with either 200 mM Na$^+$ or 200 mM K$^+$. Both double mutants showed a time-dependent drop of fluorescence only for Na$^+$-loaded liposomes, indicating the absence of K$^+$-mediated proton influx. The Na$^+$/H$^+$ exchange activity of both double mutants was reduced in comparison to WT MjNhaP1. Both experiments thus demonstrate that K$^+$ is transported neither by WT MjNhaP1 nor the double mutants A130S/P133A and A130S/P162A, despite the tuned local binding properties.

■ DISCUSSION AND CONCLUSION

In the environment of submarine hydrothermal vents, the typical habitat of *M. jannaschii*, MjNhaP1 is believed to work as Na$^+$-driven proton exporter, powered by a Na$^+$ gradient between the saline environment and the inside of the cell. MjNhaP1 uses this Na$^+$ gradient to deacidify the inside of the cell by exchanging protons from the inside against Na$^+$ ions from the outside. However, Na$^+$/H$^+$ antiporters are able to transport ions and protons in both directions, with net transport determined by the dominant chemical gradient across the membrane.

In our biophysical measurements, we found that MjNhaP1 transports Na$^+$ but not K$^+$ (Figure 1). In our MD simulations, we found that the inward-open state of MjNhaP1 strongly favors binding of Na$^+$ over K$^+$ (Figure 6). The calculated differences in ion binding affinity account for the differences in transport between Na$^+$ and K$^+$ ions seen experimentally. However, this does not exclude other contributions, in particular differential ion binding to the occluded transition state of ion transport[13] or slow on rate and/or off rates for K$^+$ ions. It is also conceivable that K$^+$ acts as an inhibitor. However, our equilibrium MD simulations suggest that K$^+$ ions dissociate rapidly, on a submicrosecond time scale, from inward-open and outward-open states. Moreover, the overall slow transport rate and the fast transition-path time for ion exchange[13] make it unlikely that K$^+$ ions trap an occluded state. Therefore, the strong preference for Na$^+$ over K$^+$ in the inward-open state and the weak preference for Na$^+$ in the outward-open state are likely to be the major determinants of Na$^+$ selectivity.

The asymmetry of the calculated ion-binding affinities is consistent with the presumed functional requirements on ion exchange in sea water. According to our free energy calculations, MjNhaP1 exhibits a strong preference for Na$^+$ over K$^+$ in the inward-open state and only a weak preference in the outward-open state. In sea water, the concentration of Na$^+$ ions is about 50 times higher than that of K$^+$ ions. Therefore, no selectivity is required for binding of Na$^+$ to the outward-open state, simply because the binding site will be overwhelmed by abundant Na$^+$ ions. Indeed, an occasional uptake of K$^+$ might actually be beneficial because the concentration of K$^+$ ions is about 10 times higher than that of Na$^+$ ions in the cytosol of most cells. To maintain this reversed concentration ratio against a strong thermodynamic driving force for K$^+$ efflux and Na$^+$ influx, it is important that the inward-open access state of MjNhaP1 is highly selective for Na$^+$ against K$^+$ ions. This strong Na$^+$ preference in the inward-open access state is supported by our atomistic MD simulations and free energy calculations. By contrast, Na$^+$ ions are relatively weakly bound

in the outward-open state, consistent with the functional requirements of a Na$^+$-driven proton export. The abundance of Na$^+$ in sea water ensures a fast on-rate even for a relatively weak binding site. Conversely, we expect that the fully exposed Asp-161 in the outward-open state will ensure a fast release of the transported protons to the outside, as another functional requirement.

Based on the molecular simulations, we could identify some of the residues responsible for ion selectivity. Our findings support the phylogeny-based hypothesis by Masrati et al.[16] that polar residues close to the binding site at transmembrane helix 4 contribute to the ion selectivity. The conservation patterns of the primary residues in Na$^+$/H$^+$ and K$^+$/H$^+$ exchangers indicate that K$^+$ selectivity results from a cumulative effect of secondary contributions. Guided by sequence comparison of antiporters with demonstrated K$^+$ ion transport, we identified residues A130 and P162. In the double mutant A130S/P162A, the calculated preference of Na$^+$ over K$^+$ in the inward-open state weakened by 2.5 kcal mol^{-1}, with a remaining preference for Na$^+$ of 2.7 kcal mol^{-1}.

The calculated ion selectivities of the WT and the double mutant are consistent with our experimental measurements. For the WT, our calculated preference for Na$^+$ binding is consistent with the absence of detectable K$^+$ transport. For the double mutant A130S/P162A, the theoretical results predict a concentration ratio of [K$^+$]/[Na$^+$] of ≈80/1 to achieve equal occupancy. By converting this difference in calculated equilibrium affinity into a difference in transport rate, one would expect a roughly 80 times slower transport of K$^+$ compared to Na$^+$, which would not be detectable with our experiments. Indeed, in our experiments, we did not detect K$^+$ transport in the A130/P162 double mutant, consistent with the theoretical prediction. Turning MjNhaP1 into a K$^+$/H$^+$ exchanger would require additional mutations, possibly involving the entire transport pathway, as resolved in atomic detail for PaNhaP by transition-path sampling.[13]

Overall, our combined experimental and computational findings show that MjNhaP1 is selective for Na$^+$ over K$^+$. The difference in binding free energies in the inward-open and outward-open states likely has functional relevance. Based on the molecular simulations, we identified residues directly responsible for Na$^+$ selectivity that are consistent with sequence conservation across the transporter family.[16] Having established ion selectivity by experiment and molecular dynamics simulations, and having quantified the contributions of several residues to ion selectivity through free-energy calculations, we set a foundation for further studies of ion selectivity in cation/proton exchangers.

ASSOCIATED CONTENT

Ⓢ Supporting Information

The Supporting Information is available free of charge at https://pubs.acs.org/doi/10.1021/acs.jpcb.9b08552.

> Tables S1−S6 and Figures S1−S4 and S6 with detailed simulation results, Figure S5 with sequence alignment, and Figure S7 with ion transport measurements on double mutant proteins (PDF)

AUTHOR INFORMATION

Corresponding Authors

*(V.R.I.K.) E-mail: ville.kaila@ch.tum.de.
*(W.K.) E-mail: werner.kuehlbrandt@biophys.mpg.de.
*(G.H.) E-mail: gerhard.hummer@biophys.mpg.de.

ORCID 🔘

Ville R. I. Kaila: 0000-0003-4464-6324
Gerhard Hummer: 0000-0001-7768-746X

Author Contributions

#These authors contributed equally to this work.

Notes

The authors declare no competing financial interest.

REFERENCES

(1) Brett, C. L.; Donowitz, M.; Rao, R. Evolutionary origins of eukaryotic sodium/proton exchangers. *Am. J. Physiol., Cell Physiol.* **2005**, *288*, C223−C239.

(2) Kondapalli, K.; Hack, A.; Schushan, M.; Landau, M.; Ben-Tal, N.; Rao, R. Functional evaluation of autism-associated mutations in NHE9. *Nat. Commun.* **2013**, *4*, 2510.

(3) Orlowski, J.; Grinstein, S. Diversity of the mammalian sodium/proton exchanger SLC9 gene family. *Pfluegers Arch.* **2004**, *447*, 549−565.

(4) Mitchell, P. A general theory of membrane transport from studies of bacteria. *Nature* **1957**, *180*, 134−136.

(5) Jardetzky, O. Simple allosteric model for membrane pumps. *Nature* **1966**, *211*, 969−970.

(6) Hunte, C.; Screpanti, E.; Venturi, M.; Rimon, A.; Padan, E.; Michel, H. Structure of a Na$^+$/H$^+$ antiporter and insights into mechanism of action and regulation by pH. *Nature* **2005**, *435*, 1197−1202.

(7) Lee, C.; Kang, H. J.; Von Ballmoos, C.; Newstead, S.; Uzdavinys, P.; Dotson, D. L.; Iwata, S.; Beckstein, O.; Cameron, A. D.; Drew, D. A two-domain elevator mechanism for sodium/proton antiport. *Nature* **2013**, *501*, 573−577.

(8) Wöhlert, D.; Kühlbrandt, W.; Yildiz, Ö. Structure and substrate ion binding in the sodium/proton antiporter PaNhaP. *eLife* **2014**, *3*, No. e03579.

(9) Paulino, C.; Wöhlert, D.; Kapotova, E.; Yildiz, Ö.; Kühlbrandt, W. Structure and transport mechanism of the sodium/proton antiporter MjNhaP1. *eLife* **2014**, *3*, No. e03583.

(10) Goswami, P.; Paulino, C.; Hizlan, D.; Vonck, J.; Yildiz, Ö.; Kühlbrandt, W. Structure of the archaeal Na$^+$/H$^+$ antiporter NhaP1 and functional role of trans membrane helix 1. *EMBO J.* **2011**, *30*, 439−449.

(11) Calinescu, O.; Paulino, C.; Kühlbrandt, W.; Fendler, K. Keeping it simple, transport mechanism and pH regulation in Na$^+$/H$^+$ exchangers. *J. Biol. Chem.* **2014**, *289*, 13168−13176.

(12) Arkin, I. T.; Xu, H.; Jensen, M.; Arbely, E.; Bennett, E. R.; Bowers, K. J.; Chow, E.; Dror, R. O.; Eastwood, M. P.; Flitman-Tene, R.; et al. Mechanism of Na$^+$/H$^+$ antiporting. *Science* **2007**, *317*, 799−803.

(13) Okazaki, K.; Wöhlert, D.; Warnau, J.; Jung, H.; Yildiz, Ö.; Kühlbrandt, W.; Hummer, G. Mechanism of the electroneutral sodium/proton antiporter PaNhaP from transition-path shooting. *Nat. Commun.* **2019**, *10*, 1742.

(14) Gierth, M.; Mäser, P. Potassium transporters in plants - Involvement in K$^+$ acquisition, redistribution and homeostasis. *FEBS Lett.* **2007**, *581*, 2348−2356.

(15) Resch, C. T.; Winogrodzki, J. L.; Patterson, C. T.; Lind, E. J.; Quinn, M. J.; Dibrov, P.; Häse, C. C. Putative Na$^+$/H$^+$ antiporter of

Vibrio cholerae, Vc-NhaP2, mediates the specific K⁺/H⁺ exchange in vivo. *Biochemistry* **2010**, *49*, 2520−2528.

(16) Masrati, G.; Dwivedi, M.; Rimon, A.; Gluck-Margolin, Y.; Kessel, A.; Ashkenazy, H.; Mayrose, I.; Padan, E.; Ben-Tal, N. Broad phylogenetic analysis of cation/proton antiporters reveals transport determinants. *Nat. Commun.* **2018**, *9*, 4205.

(17) Olsson, M. H. M.; Søndergaard, C. R.; Rostkowski, M.; Jensen, J. H. PROPKA3: consistent treatment of internal and surface residues in empirical pK_a predictions. *J. Chem. Theory Comput.* **2011**, *7*, 525−537.

(18) Søndergaard, C. R.; Olsson, M. H.; Rostkowski, M.; Jensen, J. H. Improved treatment of ligands and coupling effects in empirical calculation and rationalization of pK_a values. *J. Chem. Theory Comput.* **2011**, *7*, 2284−2295.

(19) Phillips, J. C.; Braun, R.; Wang, W.; Gumbart, J.; Tajkhorshid, E.; Villa, E.; Chipot, C.; Skeel, R. D.; Kalé, L.; Schulten, K. Scalable molecular dynamics with NAMD. *J. Comput. Chem.* **2005**, *26*, 1781−1802.

(20) Best, R. B.; Zhu, X.; Shim, J.; Lopes, P. E. M.; Mittal, J.; Feig, M.; MacKerell, A. D. Optimization of the additive charmm all-atom protein force field targeting improved sampling of the backbone Φ, Ψ, and side-chain $χ1$ and $χ2$ dihedral angles. *J. Chem. Theory Comput.* **2012**, *8*, 3257−3273.

(21) Klauda, J. B.; Venable, R. M.; Freites, J. A.; O'connor, J. W.; Tobias, D. J.; Mondragon-Ramirez, C.; Vorobyov, I.; Mackerell, A. D.; Pastor, R. W. Update of the charmm all-atom additive force field for lipids: validation on six lipid types. *J. Phys. Chem. B* **2010**, *114*, 7830−7843.

(22) Beglov, D.; Roux, B. Finite representation of an infinite bulk system: solvent boundary potential for computer simulations. *J. Chem. Phys.* **1994**, *100*, 9050−9063.

(23) Noskov, S. Y.; Roux, B. Control of ion selectivity in LeuT: two Na⁺ binding sites with two different mechanisms. *J. Mol. Biol.* **2008**, *377*, 804−818.

(24) Feller, S. E.; Zhang, Y.; Pastor, R. W.; Brooks, B. R. Constant pressure molecular dynamics simulation: the Langevin piston method. *J. Chem. Phys.* **1995**, *103*, 4613−4621.

(25) Darden, T.; York, D.; Pedersen, L. Particle mesh Ewald: an N·log(N) method for Ewald sums in large systems. *J. Chem. Phys.* **1993**, *98*, 10089−10092.

(26) Trabuco, L. G.; Villa, E.; Mitra, K.; Frank, J.; Schulten, K. Flexible fitting of atomic structures into electron microscopy maps using molecular dynamics. *Structure* **2008**, *16*, 673−683.

(27) Becke, A. D. Density-functional thermochemistry. III. The role of exact exchange. *J. Chem. Phys.* **1993**, *98*, 5648−5652.

(28) Lee, C.; Yang, W.; Parr, R. G. Development of the Colle-Salvetti correlation-energy formula into a functional of the electron density. *Phys. Rev. B: Condens. Matter Mater. Phys.* **1988**, *37*, 785−789.

(29) Weigend, F.; Ahlrichs, R. Balanced basis sets of split valence, triple zeta valence and quadruple zeta valence quality for H to Rn: Design and assessment of accuracy. *Phys. Chem. Chem. Phys.* **2005**, *7*, 3297.

(30) MacKerell, A. D.; Bashford, D.; Bellott, M.; Dunbrack, R. L.; Evanseck, J. D.; Field, M. J.; Fischer, S.; Gao, J.; Guo, H.; Ha, S.; et al. All-atom empirical potential for molecular modeling and dynamics studies of proteins. *J. Phys. Chem. B* **1998**, *102*, 3586−3616.

(31) Brooks, B. R.; Brooks, C. L., III; Mackerell, A. D., Jr.; Nilsson, L.; Petrella, R.; Roux, B.; Won, Y.; Archontis, G.; Bartels, C.; Boresch, S.; et al. CHARMM: the biomolecular simulation program. *J. Comput. Chem.* **2009**, *30*, 1545−1614.

(32) *TURBOMOLE V6.2 2010, a development of University of Karlsruhe and Forschungszentrum Karlsruhe GmbH, 1989−2007*; TURBOMOLE GmbH, since 2007; http://www.turbomole.com.

(33) Ahlrichs, R.; Bär, M.; Häser, M.; Horn, H.; Kölmel, C. Electronic structure calculations on workstation computers: the program system turbomole. *Chem. Phys. Lett.* **1989**, *162*, 165−169.

(34) Riahi, S.; Rowley, C. N. The CHARMM-TURBOMOLE interface for efficient and accurate QM/MM molecular dynamics, free energies, and excited state properties. *J. Comput. Chem.* **2014**, *35*, 2076−2086.

(35) Lev, B.; Roux, B.; Noskov, S. Y. Relative Free Energies for Hydration of Monovalent Ions from QM and QM/MM Simulations. *J. Chem. Theory Comput.* **2013**, *9*, 4165−4175.

(36) Shirts, M. R.; Chodera, J. D. Statistically optimal analysis of samples from multiple equilibrium states. *J. Chem. Phys.* **2008**, *129*, 124105.

(37) Hummer, G.; Pratt, L. R.; Garcia, A. E. Free energy of ionic hydration. *J. Phys. Chem.* **1996**, *100*, 1206−1215.

(38) Hummer, G.; Pratt, L. R.; Garcia, A. E. Ion sizes and finite-size corrections for ionic-solvation free energies. *J. Chem. Phys.* **1997**, *107*, 9275.

(39) Hünenberger, P. H.; McCammon, J. A. Ewald artifacts in computer simulations of ionic solvation and ion-ion interaction: a continuum electrostatics study. *J. Chem. Phys.* **1999**, *110*, 1856−1872.

(40) Padan, E.; Danieli, T.; Keren, Y.; Alkoby, D.; Masrati, G.; Haliloglu, T.; Ben-Tal, N.; Rimon, A. NhaA antiporter functions using 10 helices, and an additional 2 contribute to assembly/stability. *Proc. Natl. Acad. Sci. U. S. A.* **2015**, *112*, E5575−E5582.

(41) Humphrey, W.; Dalke, A.; Schulten, K. VMD: Visual molecular dynamics. *J. Mol. Graphics* **1996**, *14*, 33−38.

(42) Notredame, C.; Higgins, D. G.; Heringa, J. T-Coffee: a novel method for fast and accurate multiple sequence alignment. *J. Mol. Biol.* **2000**, *302*, 205−2017.

(43) Floden, E. W.; Tommaso, P. D.; Chatzou, M.; Magis, C.; Notredame, C.; Chang, J.-M. PSI/TM-Coffee: a web server for fast and accurate multiple sequence alignments of regular and trans-membrane proteins using homology extension on reduced databases. *Nucleic Acids Res.* **2016**, *44*, W339−W343.

(44) Waterhouse, A. M.; Procter, J. B.; Martin, D. M. A.; Clamp, M.; Barton, G. Jalview version 2-a multiple sequence alignment editor and analysis workbench. *Bioinformatics* **2009**, *25*, 1189−1191.

(45) Zhu, F.; Hummer, G. Drying transition in the hydrophobic gate of the GLIC channel blocks ion conduction. *Biophys. J.* **2012**, *103*, 219−227.

(46) Conway, B. E. Evaluation and use of properties of individual ions in solution. *J. Solution Chem.* **1978**, *7*, 721−770.

(47) Xu, Y.; Zhou, Y.; Hong, S.; Xia, Z.; Cui, D.; Guo, J.; Xu, H.; Jiang, X. Functional characterization of a wheat NHX antiporter gene TaNHX2 that encodes a K⁺/H⁺ exchanger. *PLoS One* **2013**, *8*, e78098.

(48) Radchenko, M. V.; Tanaka, K.; Waditee, R.; Oshimi, S.; Matsuzaki, Y.; Fukuhara, M.; Kobayashi, H.; Takabe, T.; Nakamura, T. Potassium/proton antiport system of Escherichia coli. *J. Biol. Chem.* **2006**, *281*, 19822−19829.